Int. J. Electrochem. Sci., 11 **(2016)** 6423 – 6431, doi: 10.20964/2016.08.36

International Journal of ELECTROCHEMICAL SCIENCE
www.electrochemsci.org

Growth Mechanism of Electrodeposited Fe, Co and Ni Nanowires in the Form of Self-Assembled Arrays at Fixed Potential

Tahir Mehmood[1,*], *Aiman Mukhtar, Babar Shahzad Khan, Kaiming Wu*[2,*]

The State Key Laboratory of Refractories and Metallurgy, Hubei Province Key Laboratory of Systems Science in Metallurgical Process, International Research Institute for Steel Technology, Wuhan University of Science and Technology, Wuhan 430081, P. R. China
E-mail: tahir10621@yahoo.com, wukaiming@wust.edu.cn

Received: 28 January 2016 / *Accepted:* 25 April 2016 / *Published:* 7 July 2016

The growth mechanism of electrodeposited Fe, Ni and Co nanowires has been investigated by X-ray diffractometry, scanning electron microscopy and electrochemistry. It is found that the current density for deposition of Fe nanowires is higher than that of Co and Ni nanowires under the same overpotential, pH, concentration of metal ions and temperature. Using the electron tunneling theory, this phenomenon has been ascribed to the higher charge transfer coefficient of Fe than that of Co and Ni.

Keywords: Nanostructure; electrodeposition; current density; work function

1. INTRODUCTION

Understanding various factors that influence the growth of electrodeposited metal nanowires is of scientific and technological interests. Deposition potential plays an important role in controlling the metal nanowire growth. For example, the nanowires of Au, Ag, and Cu are single crystalline under the low deposition potential, and polycrystalline under the high deposition potential [1]. Phase selection could also be realized by varying deposition potential: studies of Wang et al [2] and Huang et al [3] show that the single crystalline Co nanowires are hcp (hexagonal close packing) phase at the lower deposition potential of about -1.5 V, and fcc (face-centered cubic) phase at the higher deposition potential of -3.0 V. Darques et al reported that an appropriate pH of electrolytic solution, combined with current density, can control the orientation of the hcp *c* axis in Co nanowires with respect to the

wire axis [4]. Details of the effect of deposition parameters on phase transformation are given in our previous work [5,6]. S. L. Diaz et al presented the kinetics of Fe electrodeposition as a function of solution pH by means of polarization curves in sulphate solution [7], but growth mechanism of metal nanowires through electrodeposition is still an enigma.

The growth of metal nanowires can be pictured as the four steps at the atomic-level scale[8]. The dehydration of hydrated metal ions can be the most important among the four steps. The dehydration involves valence electrons tunneling to hydrated metal ions[8, 9], leading to neutralization of the hydrated metal ions. The neutral metal atoms are adsorbed on the surface and then diffuses to surface sites (such as kink site) where they incorporate into the metal lattice, thus leading to the growth.[8] Therefore, the growth rate is related by the dehydration[8]. Since the probability of electron tunneling is related to the work function of metals, the work function can have a significant effect on the growth of metal nanowires. Moreover, the elemental processes of electrodeposition are still not well understood. The aim of this work is to study the work function effect of metal nanowire growth and to understand the electrode reaction mechanism.

2. EXPERIMENTAL DETAILS

The porous anodic alumina membranes (AAM) templates were prepared using a two-step anodization procedure [10,11]. Here we briefly describe the experimental procedure as shown in Fig. 1.

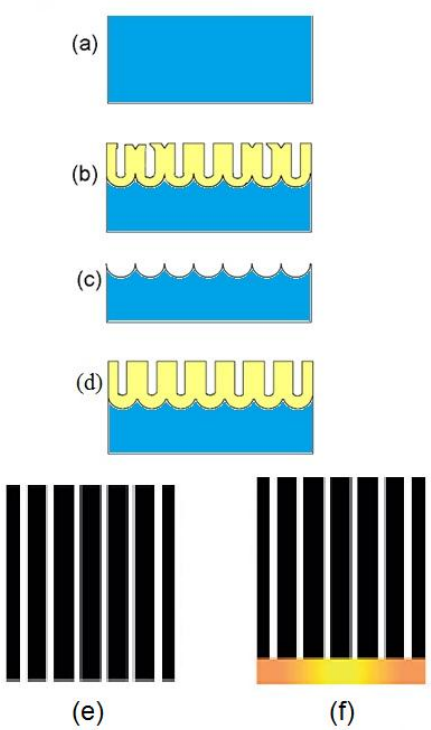

Figure 1. Schematic view of the process flow used for AAO template formation (a) Al foil (b) first anodization step (c) removal of first AAO layer, (d) second anodization step and AAO membranes; before gold sputtering (e), and after gold sputtering (f)

Firstly, high-purity aluminum foils (99.999%) were degreased in acetone and then were annealed in a vacuum of 10^{-5} Torr at 500^0C for 5 h to remove the mechanical stress. Secondly, the aluminum foils were anodized in a 0.3 M $H_2C_2O_4$ solution at 2^0C for 6 h. After removing the alumina layer formed in the anodization in a mixture of phosphoric acid (6 wt %) and chromic acid (1.8 wt %), the aluminum foils were anodized again at the same conditions as the first anodization for 12 h. The templates that experienced the above two-step anodization were etched in a saturated $CuCl_2$ solution to remove the remaining aluminum on the back side. Thirdly, the alumina barrier layer was then dissolved in a 5 wt% phosphoric acid solution at 40^0C. The templates obtained by the above method have the cylindrical and hexagonally arranged pores of about 50 nm. Finally, a gold film was sputtered onto the back side of the templates to serve as the working electrode.

The electrolytes have the same concentration of metal ions. The electrolyte was 0.536M $FeSO_4 \cdot 7H_2O$ and 0.72M H_3BO_3 for deposition of Fe nanowires, 0.536M $CoSO_4 \cdot 7H_2O$ and 0.72M H_3BO_3 for deposition of Co nanowires and 0.536M $NiSO_4 \cdot 6H_2O$ and 0.72M H_3BO_3 for deposition of Ni nanowires. The pH of the two as-prepared solutions was adjusted to 2 by adding 1M H_2SO_4 solution. Direct current electrodeposition (shown in Fig. 2) was conducted in a three-electrode cell at room temperature.

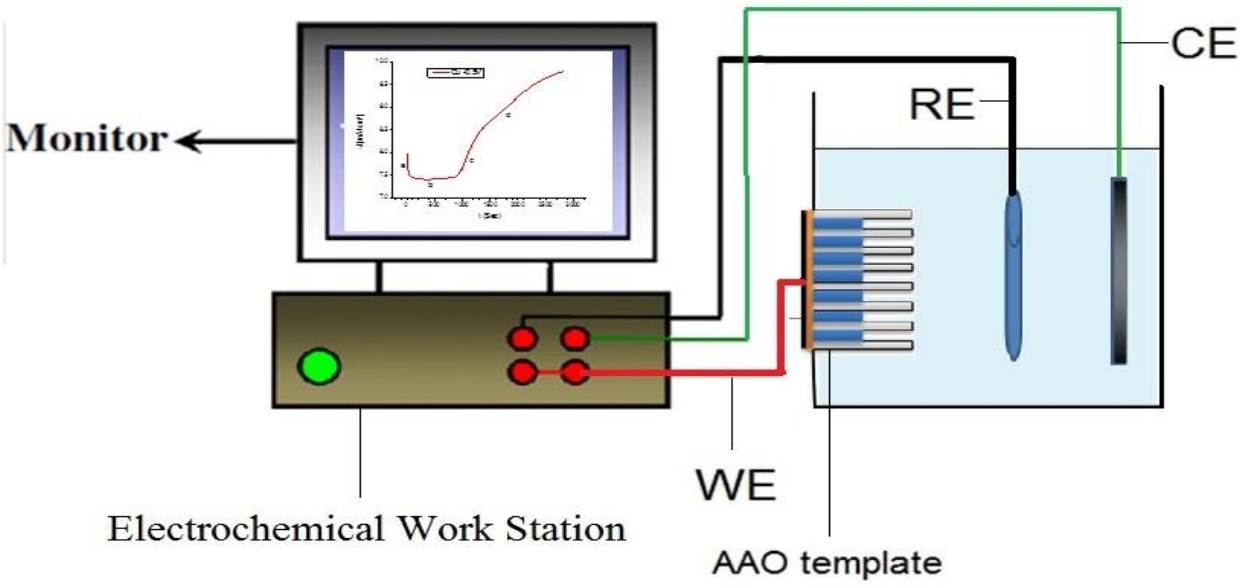

Figure 2. Schematic representation of a three electrode electrochemical cell

The area of the working electrode for growth of nanowires was 0.608cm^2 ($=0.25\pi(0.88cm)^2$) and the area of the graphite counter electrode was 14.7cm^2 ($=4.2cm\times3.5cm$). The reference electrode was the saturated calomel. The Co and Ni nanowires were analyzed by X-ray diffraction (XRD, Y-2000) with CuK_α radiation. Before XRD measurements the sputtered Au film was mechanically polished away. The deposited Fe, Co and Ni nanowires were also examined by scanning electron microscope (SEM, JEOL JSM-6700F). In order to perform SEM observations, the AAO template was

partly dissolved with a 5 wt% NaOH solution, and then carefully rinsed with deionized water for several times.

3. RESULTS AND DISCUSSION

The deposition current density represents the growth rate of metal nanowires. The higher the current density is, the faster the growth rate is. The relationship between the current density (i) and the overpotential (η) is given by [12],

$$\eta = a + b \log i \quad (1)$$

$$\eta = E(I) - E \quad (2)$$

Where a and b are constants, $E(I)$ is the potential applied to the electrode, E is the equilibrium potential of the electrode (the potential in the absence of external current). E is identical to the open circuit potential since there is no external current at the open circuit potential. In order to study the effect of work function on the growth rate of metal nanowires, two experimental conditions are satisfied. First, metal nanowires are deposited at the same overpotential, pH, concentration of metal ions and temperature, since they have an influence on the current density. Second, the deposition is divided into two steps. The reason for this is as follows. The E of eq. (2) is actually the equilibrium potential (or the open circuit potential) of the deposited metal. The initial working electrode is not the electrodeposited metal but the sputtered Au film. For the first step deposition, Fe, Co and Ni were deposited at -0.9V with respect to the reference electrode for 10 min separately. After the first step deposition, the open circuit potential of Co and Ni nanowires was determined to be -0.48V (SCE) and -0.34V (SCE), respectively. Subsequently, the deposition was again conducted at a chosen overpotential ($\eta = E(I) - E$, where E (I) is the applied potential and E is the open circuit potential).

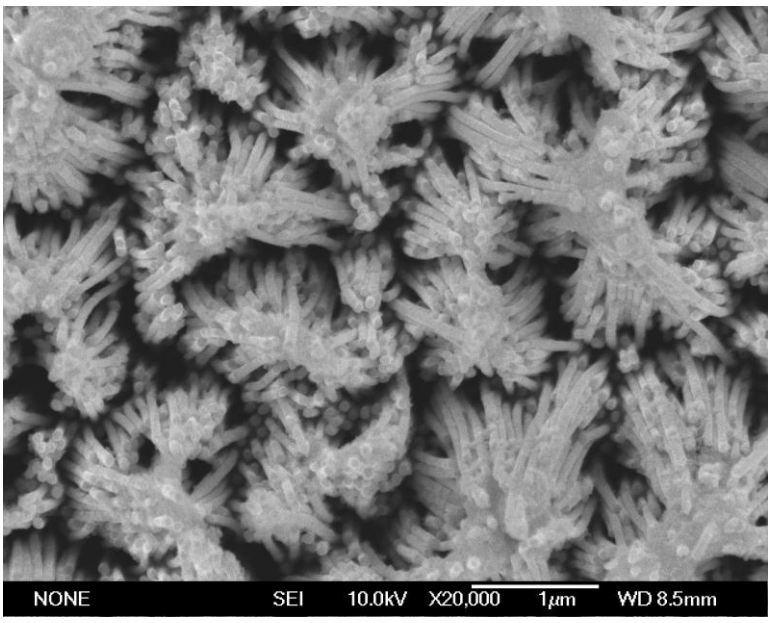

Figure 3. SEM image of Fe nanowires deposited at -0.9 V

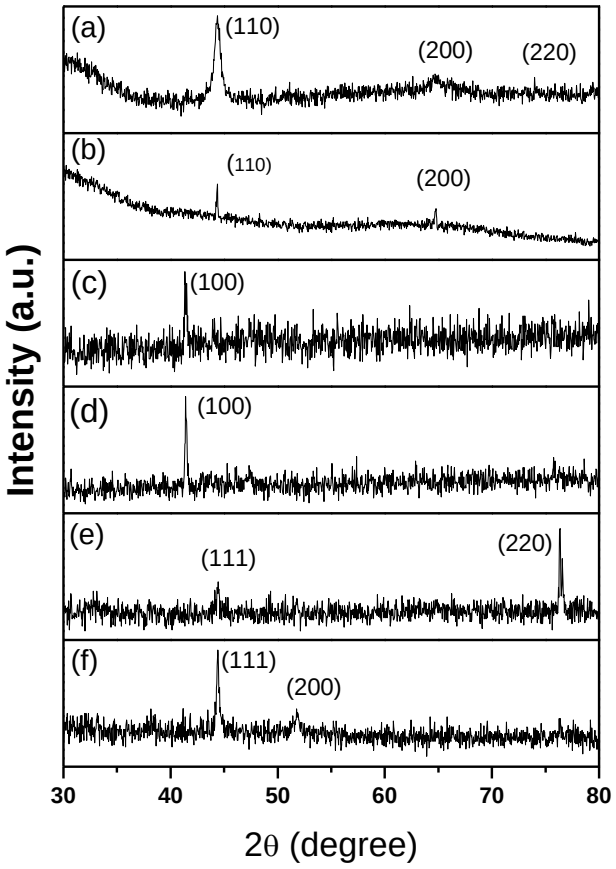

Figure 4. X-ray diffraction (XRD) patterns of Fe, Co and Ni nanowires: (a) Fe at -0.9V, (b) Fe at -0.6V, (c) Co at -0.9V, (d) Co at -0.6V, (e) Ni at -0.9V and (f) Ni at -0.6V.

Fig. 3 shows the SEM image of Fe nanowires. The diameter of Fe nanowires (~50 nm) is the same as that of the pores of AAO template (~50nm), indicating that the cylindrical pores of the AAO template were fully filled with Fe metal atoms during electrodeposition.

Fig. 4 shows the X-ray diffraction (XRD) patterns of Fe, Co and Ni nanowires deposited at overpotential of -0.6 and -0.9V, respectively. The XRD data were collected from the top side of nanowires. The Fe nanowires deposited at -0.6V and -0.9V have cubic structure and the preferential growth is on the (110) plane. The Co nanowires deposited at -0.6 and -0.9V are hcp phase. The preferential growth plane is on the $(10\bar{1}0)$. The Ni nanowires deposited at -0.6 and -0.9V are fcc phase. The preferential growth plane is on the (111) and (110) for Ni nanowires deposited at -0.6V and -0.9V, respectively.

Figs. 5 and 6 show the current density against time curves measured in the second-step deposition of Fe, Co and Ni nanowires at the overpotential (η) of -0.9V and -0.6V respectively. The averaged current density at -0.9V is 11.47 mA/cm^2 for Fe, 8.34 mA/cm^2 for Co, 4.92mA/cm^2 for Ni, and at -0.6V is 5.41 mA/cm^2 for Fe, 3.33mA/cm^2 for Co and 1.61mA/cm^2 for Ni. We can see two interesting points from Figs. 5 and 6 that under the same η, pH, concentration of metal ions and

temperature, the current density of deposition of Fe is higher than that of Co and Ni, indicating that Fe nanowires grow faster than Co and Ni nanowires. The explanation for this is as follows.

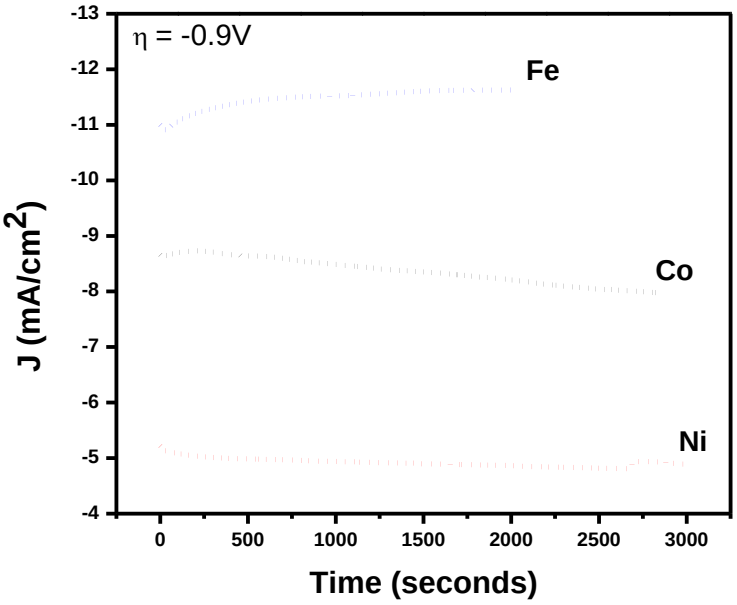

Figure 5. Current density vs time curves measured in the second-step deposition of Fe, Co and Ni nanowires at -0.9V

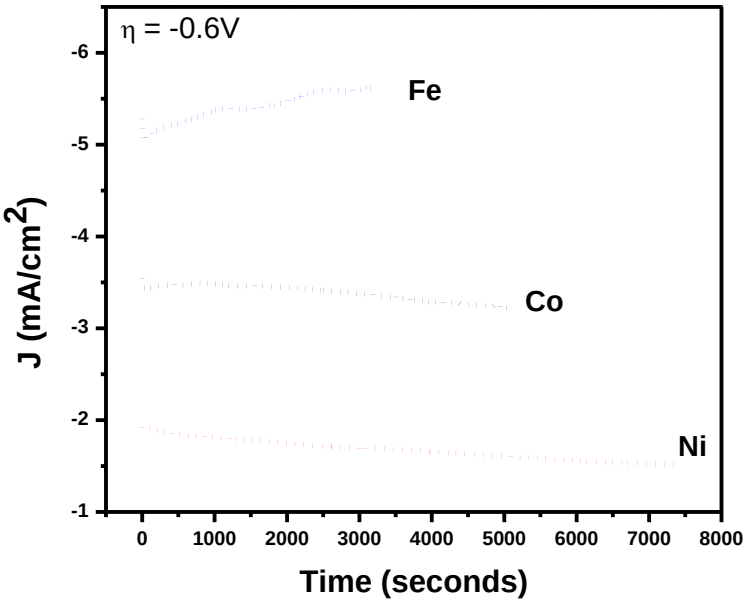

Figure 6. Current density vs time curves measured in the second-step deposition of Fe, Co and Ni nanowires at -0.6V

The relationship between the current density and the overpotential is described by the Bulter–Volmer equation[12]. For the large negative values of overpotential like -0.6 and -0.9V, the Bulter–Volmer equation can be approximated by [12].

$$i = -i_0 \exp\left(-\frac{\alpha z F \eta}{RT}\right) \quad (3)$$

where i, the current density, i_0, the exchange current density, α, the charge transfer coefficient, z, the valence of deposited metal ions, F, the Faraday constant, η, the overpotential, R, the gas constant, and T is the absolute temperature. Exchange current density of Ni is approximately the same as that of Co at pH 2.5[13]. The valence of deposited Ni and Co ions, which is 2+, is also the same. Consequently, the current density (i) depends only on the charge transfer coefficient (α) and increases with increasing α. Here we will elucidate using the electron tunneling theory that the charge transfer coefficient of Co (α_{Co}) is higher than that of Ni (α_{Ni}).

Electron tunneling is used to describe electronic processes arising near metal surface. When positively charged ions approach a metal surface, these ions can be neutralize by metal valence electrons via electron tunneling. In case of low-energy ion scattering experiments, low energy ions which are incident on a metal surface are neutralized through electron tunneling[14]. In electrodeposition process, metal valence electrons can also tunnel to dehydrated metal ions, leading to neutralization[8, 9]. This is because the wave function of valence electrons in metals does not drop to zero abruptly at the surface but prolong above the surface with an exponentially decaying tail[15]. When the wave function tail of the valence electron overlaps with the orbital wave function of hydrated metal ions, the valence electron can tunnel to vacant orbital of hydrated metal ions. As a first approximation, the tunneling probability is mostly resolute by the overlap of the wave functions. The larger the overlap between the orbital wave function and the valence electron wave function is, the larger the tunneling probability is. This overlapping depends very perceptively on the extension of decaying tail and the distance of hydrated metal ions from surface.

The wavefunction of electrons above the surface decays exponentially according to [16]

$$\psi \propto e^{-0.51\sqrt{\phi}\cdot d} \quad (4)$$

Where *d* is the distance from metal surface in Å and the workfunction Φ in eV. Since the work function of polycrystalline Fe (4.67eV) is smaller than that of polycrystalline Co (5.0eV) and polycrystalline Ni (5.15eV) [17] the valence electron wavefunction of Fe decays less abruptly and prolongs more beyond the surface than that of Co and Ni. It is well understood that the structure of hydrated Co and Ni ions is octahedron[18]. When hydrated Co and Ni ions approach to and arrive at metal surface, the structure of hydrated metal ions is distorted by electron gas at metal surface. In this case, the distance of hydrated Co and Ni ions from surface should be same. Consequently, the wave function overlap depends strongly on the extension of metal wave function. Because the wave function of Co extends more above the surface than that of Ni, the overlap of Co metal wave function with the orbital wave function of hydrated Co ions is larger than the overlap of Ni metal wave function with hydrated Ni ions. Therefore the probability of Co metal valence electron transferring to hydrated Co ions will be higher than that of Ni metal valence electron transferring to hydrated Ni ions. This leads to

a higher charge transfer coefficient of Co. As a result, the current density for deposition of Co is higher than that of Ni and the current density of Fe is higher than that of Co.

The potential energy E of electrons outside of the metal differs with the field strength ε simply as $E = e \cdot \varepsilon \cdot x$, as shown in the right side of Fig.7a.

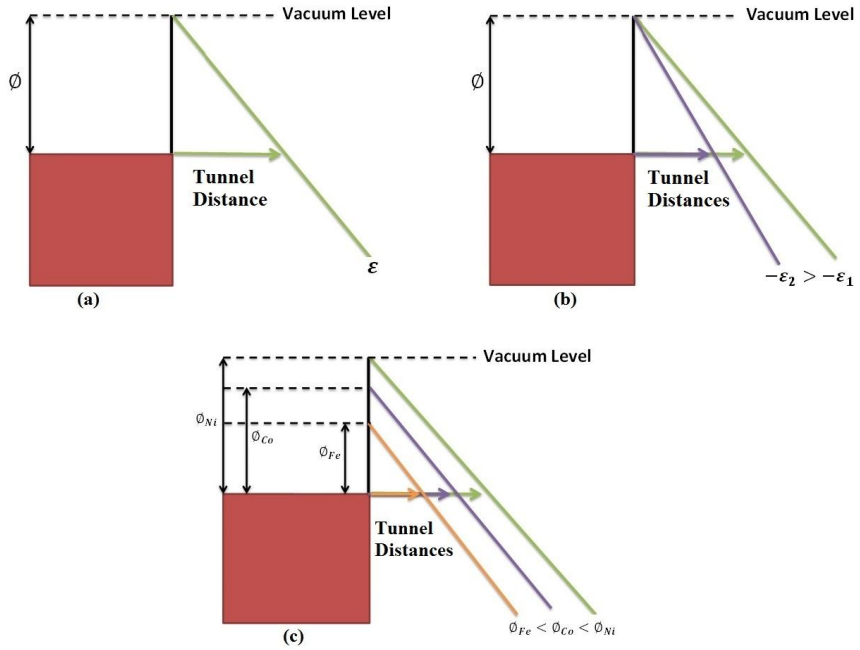

Figure 7. Schematic diagram of field emission barrier. The height of the potential barrier is determined by the workfunction of the metal ø and slope below the vacuum level shows the applied electric field ε and the electron tunneling will occur at or near the Fermi level (a), dependence of the barrier width on applied electric field (b), width of potential barrier for different work functions (c).

It is well-known that the applied potential is directly related to the current density, increasing the applied potential increases the current density. This leads to the more quick variation of the potential of electrons outside the metal, as shown in Fig.7b. In this case, the slope of electron potential with a higher electric field is steeper than that of a small electric field. The barrier width becomes thinner and electron tunneling occurs with no trouble. Hence, the current density increases with increasing the applied potential. The work function of metal can have an influence on the width of barrier through which electron tunnel. Fig. 7c shows that under the same applied potential (meaning that there is the same electric field strength in the double layer) the barrier width for the metal with small work function becomes thinner and electron tunneling takes place more easily. That's why, under the same applied potential, there is a higher current density for electrodeposition of nanowires of the metal with a smaller work function.

Our findings of current study are in good agreement of previous work of electrodepositing Ag and Cu nanowires [19]. The reasons why the current density for electrodeposition of Ag nanowires is considerably higher than that of Cu nanowires have two facts. Firstly, hydrated Ag ions are nearer to surface than hydrated Cu ions. This can meaningfully raise the current for the reason that the tunneling

current increases exponentially with the decreasing distance of hydrated metal ions from surface. Secondly, the workfunction of Ag (4.26eV) is smaller than that of Cu (4.65eV). The smaller workfunction makes the wavefunction of Ag metal have a larger overlap with orbital wavefunction of Ag+ ions, consequently increasing the tunneling current.

4. CONCLUSIONS

The current density of depositing Fe nanowires is higher than that of depositing Co as well as Ni nanowires under the same overpotential, pH, concentration of metal ions and temperature. This can be attributed to the smaller work function of Fe metal, compared to that of Co and Ni. For the surface with a smaller work function, the wave function of valence electron extends more above the surface. This causes a larger probability of electron transferring from Fe surface to hydrated Fe ions, leading to a higher charge transfer coefficient and so a higher current density.

References

1. M.L. Tian, J.G. Wang, J. Kurtz, T.E. Mallouk, and M.H.W. Chan, *Nano Lett*., 3 (2003) 919.
2. X.W. Wang, G.T. Fei, P. Tong, X.J. Xu, and L.D. Zhang, *J. Cryst. Growth.*, 300 (2007) 421.
3. X.H. Huang, L. Li, X. Luo, X.G. Zhu, and G.G. Li, *J. Phys. Chem*. C, 112 (2008) 1468.
4. M. Darques, L. Piraux, A. Encinas, P. Bayle-Guillemaud, A. Popa, and U. Ebels, *Appl. Phys. Lett.*, 86 (2005) 072508.
5. T. Mehmood, B. Shahzad Khan, A. Mukhtar, X. Chen, P. Yi, and M. Tan, *Mater. Lett.*, 130 (2014) 256.
6. T. Mehmood, B.S. Khan, A. Mukhtar, and M. Tan, *Int. J. Mate. Res.*, 106 (2015) 957.
7. S. Diaz, J. Calderón, O. Barcia, and O. Mattos, *Electrochim. Acta.*, 53 (2008) 7426.
8. M. Tan, and X.Q. Chen, *J. Electrochem. Soc*., 159 (2012) K15.
9. S.K. Lower, Electrochemistry, Simon Fraser University, Textbook.
10. H. Masuda, and K. Fukuda, *Science*, 268 (1995) 1466.
11. X.W. Wang, G.T. Fei, L. Chen, X.J. Xu, and L.D. Zhang, *Electrochem. Solid Sate.*, 10 (2007) E1.
12. M. Paunovic, M. Schlesinger, Fundamentals of Electrochemical Deposition, Wiley, New York, 1998.
13. H. Kita, *J. Electrochem. Soc.*,113 (1966) 1096.
14. J.C. Tully, N.H. Tolk, in: J.C.T. N.H. Tolk, W. Heiland, C.W. White (Ed.) Inelastic Particle-Surface Collision, Academic Press INC, New York, 1977, pp. 105.
15. L.E.C.v.d. Leemput, and H.v. Kempen, *Rep. Prog. Phys.*, 55 (1992) 1165.
16. S.J. Garrett, Introduction to Surface Analysis, the Michigan State University, Chemistry Department, East Lansing.
17. J. Speight, Lange's Handbook of Chemistry, 16th ed ed., McGraw-Hill Professional, Boston, MA, 2004.
18. I. Persson, *Pure Appl. Chem*., 82 (2010) 1901.
19. B. Shahzad Khan, A. Mukhtar, T. Mehmood, and M. Tan, *J. Nanosci. Nanotecnnol*, 16 (2016) 1.